Evolution of firework-related barium aerosols: insights from single-particle analysis and mass concentration monitoring

Xiufeng Lian[1, 2], Chenglei Pei[3], Wei Sun[4], Chen Lv[5], Kunlun Huang[3], Lei Lei[3], Bo Huang[2], Chunlei Cheng[1], Guohua Zhang[4], Xinhui Bi[4], Zhen Zhou[1], Mei Li[1,*]

[1] College of Environment and Climate, Institute of Mass Spectrometry and Atmospheric Environment, Guangdong Provincial Engineering Research Center for On-line Source Apportionment System of Air Pollution, Jinan University, Guangzhou 510632, China

[2] Guangzhou Hexin Instrument Co., Ltd., Guangzhou 510530, China

[3] Guangzhou Sub-branch of Guangdong Ecological and Environmental Monitoring Center, Guangzhou 510006, China

[4] State Key Laboratory of Organic Geochemistry and Guangdong Provincial Key Laboratory of Environmental Protection and Resources Utilization, Guangzhou Institute of Geochemistry, Chinese Academy of Sciences, Guangzhou 510640, China

[5] College of Ecology and Environment, Zhengzhou University, Zhengzhou 450001, China

[*]Correspondence to: Mei Li (*limei@jnu.edu.cn)*

Abstract. Fireworks are a well-known source of barium (Ba) in the atmosphere, yet the aging of firework-derived Ba-containing particles remain poorly understood. Combining online measurements of Ba mass concentrations with single-particle aerosol mass spectrometry (SPAMS) at four sites in Guangzhou, China, we found that firework events raised atmospheric Ba concentrations to levels 1–3 orders of magnitude above background. Peak Ba concentrations varied substantially among sites. Despite its substantially higher population density, the urban-core site under a complete firework ban exhibited a lower peak Ba concentration than a suburban site with time- and location-restricted firework use. This contrast was consistent with a potential mitigating influence of stricter controls, although site-specific emissions and transport may also have contributed. Among the identified particle classes, chloride-rich OClN particles and nitrate-dominated N particles were interpreted as relatively early and more advanced stages of atmospheric aging, respectively. Al/Mg-containing components, were more prevalent in OClN particles than in N particles, consistent with physical mixing during early aging, while several-hour lags between OClN and N peaks and between NO_2 and particulate NO_3^- suggested secondary nitrate formation, although primary nitrate emissions from fireworks could not be excluded. These findings provide insights into the rapid aging mechanisms of firework-derived Ba particles and highlight the need to consider differentiated firework-control measures alongside site-specific emission and transport conditions when interpreting spatial pollution contrasts. Screening-level hazard quotients (HQs) based on an oral reference dose (RfD) surrogate were below 1, but short-duration Ba concentration peaks warrant further evaluation of their potential inhalation-related health implications using inhalation-specific toxicity benchmarks.

1 Introduction

Barium (Ba) is a potentially toxic element whose health effects depend strongly on its chemical form (Kaur and Parkash, 2022; Sharma and Thakur, 2025). In the atmosphere, Ba originates from both natural sources (e.g., mineral dust, volcanic emissions) and anthropogenic activities (Inomata et al., 2009). Among anthropogenic sources, fireworks represent a major episodic contributor during global celebrations such as New Year's Eve, Diwali, and the Chinese Spring Festival (Hu et al., 2015; Kong et al., 2015; Lee et al., 2023). During these events, fireworks can contribute up to 87% of ambient Ba, leading to concentrations several to thousands of times higher than background levels (Hu et al., 2015; Huang et al., 2024; Kulshrestha et al., 2004; Salma et al., 2023; Tanda et al.,2019; Wang et al.,2024). This pronounced transient signal makes Ba an effective tracer for firework-derived pollution (Wang et al., 2024), providing a unique opportunity to study the atmospheric processing of metal-containing aerosols.

Fireworks are complex pyrotechnic mixtures containing oxidizers (e.g., $KClO_3$, $KClO_4$, $Ba(NO_3)_2$), fuels (e.g., sulfur, charcoal, aluminum), and colorants that produce specific metal emissions (Webster, 1985). For green fireworks, Ba compounds such as $BaCl_2$, $Ba(NO_3)_2$, and $Ba(ClO_3)_2$ are commonly used as colorants, with $BaCl_2$ being the most widely employed due to its intense green emission and favorable combustion properties (Li et al., 2013; Wang et al., 2007). Upon ignition, these Ba salts are rapidly vaporized and subsequently condense to form primary particles, which are initially enriched in chlorine (e.g., $BaCl_2$) or, depending on the formulation, in nitrate or perchlorate (Wang et al., 2007).

Despite the well-documented surge in Ba concentrations during firework events, the chemical speciation of ambient Ba-containing particles remains poorly understood and debated (Li et al., 2013; Wang et al., 2007; Webster et al., 1985). While fresh firework emissions are typically chlorine-rich (e.g., $BaCl_2$), field observations often report aged particles enriched in sulfur rather than chlorine, suggesting atmospheric transformation during transport (Li et al., 2013; Wang et al., 2007). For firework-generated particles (e.g., potassium-containing), both sulfation and nitration have been observed during aging (Wang et al., 2024). However, whether analogous transformations occur for Ba-containing particles remains largely unexplored. In this study, we investigate the aging mechanisms of firework-generated Ba aerosols from a single-particle perspective, with a focus on nitrate-mediated pathways.

The environmental and health impacts of firework-derived Ba are fundamentally governed by its chemical speciation (Inomata et al., 2009). Soluble forms such as $BaCl_2$ and $Ba(NO_3)_2$ are highly bioavailable and pose acute toxicity risks upon inhalation (Kaur and Parkash, 2022), whereas insoluble species like $BaSO_4$ exhibit low chemical toxicity but contribute to long-range transport as fine suspended particles (Inomata et al., 2009; Sharma and Thakur, 2025). Given that atmospheric aging processes, including heterogeneous reactions, gas-to-particle conversion, and physical coagulation, can fundamentally alter the chemical speciation of aerosol particles (Zhang et al., 2015), understanding how these processes apply to Ba-containing particles is essential for predicting their environmental fate and health impacts. For metal-containing particles, aging can involve the uptake of acidic gases such as NO_2 and HNO_3, leading to the formation of nitrates on particle surfaces (Liu et al., 2017; Peng

et al., 2021).

To address these knowledge gaps, we conducted continuous online monitoring of aerosols in Guangzhou, China, over a one-month period spanning the Chinese Spring Festival and Lantern Festival of 2024, using online Ba mass concentrations measurements and single-particle aerosol mass spectrometry (SPAMS). This approach allows us to obtain high temporal resolution data on the chemical composition and size distribution of Ba-containing particles at the single-particle level, as well as mass concentrations of Ba in $PM_{2.5}$. Leveraging these high-resolution measurements, we systematically investigated the variations of Ba aerosols in relation to firework events, elucidated the aging mechanisms of Ba-containing particles in the ambient atmosphere, and provided a preliminary assessment of their potential health implications based on mass concentration data. This study contributes to a more comprehensive understanding of the atmospheric fate of firework-derived metal aerosols and their potential health implications, with relevance to air quality management and public health policy in regions where fireworks are traditionally used.

2 Field measurements

2.1 Sampling sites and period

This study was conducted in Guangzhou, China, from 1 to 29 February, 2024, covering the key periods of legal fireworks use during the Chinese Spring Festival (9–10 February) and Lantern Festival (24 February). Fireworks management followed the tiered control policy of the Guangzhou Fireworks and Firecrackers Safety Management Regulation, which designates central urban districts as prohibited zones and peripheral districts as restricted zones where fireworks are permitted only during specified periods (Guangzhou Municipal People's Government, 2021).

Four monitoring sites were established across Guangzhou: Conghua Liangkou (CHLK; 23.74° N, 113.78° E), a sparsely populated area serving as an urban background site; Gongyuanqian (GYQ; 23.13° N, 113.25° E) in Yuexiu District, a prohibited zone in the central urban area; and Panyu University City (PYDXC; 23.05° N, 113.39° E) and Nansha Puzhou (NSPZ; 22.77° N, 113.60° E) in restricted zones of Panyu and Nansha districts, respectively. Although both PYDXC and NSPZ are located in restricted firework zones, their regulatory policies differ. In Panyu, fireworks are permitted only in four designated towns (Shiqi, Xinshao, Hualong, and Shilou) during the Spring Festival and Lantern Festival periods. In contrast, Nansha permits fireworks in all areas outside its prohibited zones, with a longer permitted time window covering the Spring Festival and Lantern Festival holidays.

2.2 Data analysis and presentation strategy

Hourly concentrations of trace metals, including Ba, were measured using an online ambient metal monitor (Xact 625i, Cooper Environmental) based on energy-dispersive X-ray fluorescence (Twohy et al., 2010). Water-soluble ions (NO_3^-, SO_4^{2-}, NH_4^+, Cl^-) were quantified by an online ion chromatography system (Metrohm, 6080). Single-particle chemical composition in the 0.1–2.0 μm size range was characterized in real-time by a SPAMS (Hexin Analytical Instrument Co., Ltd., Guangzhou, China).

The SPAMS system size-focuses particles via an aerodynamic lens, sizes them with two continuous 532 nm Nd:YAG lasers, and analyzes composition by laser desorption/ionization with a 266 nm pulsed laser, followed by bipolar time-of-flight mass spectrometry to obtain both positive and negative mass spectra (Li et al., 2011). Meteorological parameters (temperature and relative humidity) and concentrations of regulated gases (NO_2, SO_2, and O_3) and $PM_{2.5}$ were obtained at hourly resolution from monitoring sites co-located with the SPAMS sampling sites. All online instruments underwent regular calibration and quality assurance checks throughout the campaign. Data were synchronized to Beijing time (UTC+8) and processed as hourly averages for subsequent analysis. To account for differences in instrument performance across the four sites, particle counts were regionalized by averaging site-specific fractions and multiplying by the total particle count across all sites. Gaseous pollutants and compositional fractions were directly averaged across the four sites as arithmetic means.

2.3 Single-particle data analysis

Single-particle data were processed using MATLAB with the COCO toolkit (v3.0). Across the sites, 71,392–1,347,245 particles with valid bipolar mass spectra were detected, showing a significant correlation between total detected particle counts and $PM_{2.5}$ mass concentrations ($r = 0.682–0.767$, $p < 0.01$; **Fig. S1**), indicating that the particles detected in this study are representative of the variation trends of $PM_{2.5}$. Ba-containing particles were identified by ion signals exceeding a threshold of >5 counts (>3 times the noise level) at the characteristic mass-to-charge ratio (*m/z*) of 138 peak ([Ba^+]), yielding 679–59,010 particles (1.0–4.4% of total). These particles were clustered using the Adaptive Resonance Theory algorithm (ART-2a) based on spectral similarity in both positive and negative ion modes (Song et al., 1999), with a vigilance factor of 0.75, a learning rate of 0.05, and 20 iterations. Particles were initially grouped into 6–17 clusters based on both cationic and anionic composition (**Table 1**), whose average mass spectra are shown in **Fig. S2**. These clusters were named according to their dominant cation and anion signatures (e.g., Ba-N for nitrate-dominated clusters with Ba as the dominant cation, Al-Mg-N for nitrate-dominated clusters additionally containing Al and Mg). For interpretation of atmospheric processing, these clusters were then manually consolidated into four major categories: OClN (rich in oxygen, chloride, and nitrate), N (nitrate-dominated), NS (nitrate and sulfate internally mixed), and S (sulfate-dominated). Notably, high-molecular-weight organic matter (HMOC) interference, characterized by dense high-mass ion clusters, was observed at the CHLK site (**Fig. S3a**). These particles were separated before classification to ensure robustness. The relative peak area (RPA), defined as the fractional peak area of each *m/z* peak relative to the sum of peak areas in the mass spectrum (Healy et al., 2013; Lian et al., 2021), was used to quantify the relative abundance of chemical species in a particle.

2.4 Episode definition

The sampling period was segmented into five phases based on pronounced fluctuations in Ba mass concentration, combined with known firework activity periods, yielding two firework episodes and three background periods: Fireworks Episode I (FI)

from 9 February 17:00 to 19 February 10:00, encompassing the Spring Festival period; Fireworks Episode II (FII) from 25 February 00:00–17:00, corresponding to the Lantern Festival; and three Background periods (BI, BII, BIII) characterized by low and stable Ba concentrations. This segmentation is supported by concurrent enhancements in $PM_{2.5}$ and established firework tracers (K^+, Cl^-; **Fig. S4**) during firework episodes, establishing a robust framework for comparative analysis of firework-impacted versus background aerosol conditions. In this study, nighttime hours (19:00–05:00) were defined as the active firework emission period, and daytime hours (06:00–18:00) as the post-firework aging period.

2.5 Preliminary exposure and risk assessment methodology

To provide a preliminary screening-level assessment of potential health implications from firework-derived Ba based on mass concentration data, we estimated a surrogate inhalation dose using the USEPA framework. As no inhalation reference concentration (RfC) is available for Ba, the oral reference dose (RfD) was used as a surrogate. We acknowledge that this substitution may introduce uncertainty regarding inhalation-specific bioavailability. The average daily exposure dose (D_{inh}, $mg \cdot kg^{-1} \cdot day^{-1}$) was calculated as following the USEPA framework adapted from Kong et al. (2015), with period-specific parameters:

$$D_{inh} = \frac{C \times InhR \times EF \times ED}{BW \times AT}$$

where C is the mean hourly Ba mass concentration during each period (e.g., FI, BI). Inhalation rate (InhR) is 7.6 $m^3 \cdot day^{-1}$ for children and 20 $m^3 \cdot day^{-1}$ for adults. Exposure frequency (EF) is set to the actual duration of each period (e.g., approximately 9 days for FI) for period-specific averaging. Exposure duration (ED) is 1 year for the purpose of period-specific averaging. Body weight (BW) is 15 kg for children and 70 kg for adults. Averaging time (AT) for non-carcinogens is ED × 365 days. This approach is intended to provide a relative comparison of exposure potential between firework-impacted and background periods, rather than to estimate the absolute annual exposure risk.

The hazard quotient (HQ) for non-carcinogenic risk was calculated as:

$$HQ = \frac{D_{inh}}{RfD}$$

where RfD is the oral reference dose for Ba (0.2 $mg \cdot kg^{-1} \cdot day^{-1}$) established by the U.S. EPA Integrated Risk Information System (IRIS, 2006). HQ ≤ 1 indicates low or acceptable risk, while HQ > 1 suggests potential non-carcinogenic health effects.

3 Results and discussion

3.1 Physicochemical characteristics and spatial distribution of Ba-containing particles

3.1.1 Temporal variations of Ba mass concentration and Ba-containing particle counts

Based on comprehensive observations from the four sites, fireworks were identified as the dominant aerosol source during the study period. During FI, Ba mass concentrations increased by 17- to 40-fold, while K^+ (9- to 23-fold), Cl^- (2- to 3-fold), and heavy metals such as Cu (2- to 14-fold) and Pb (2- to 3-fold) also rose simultaneously (**Table 2, Figs. 1 and S4**). $PM_{2.5}$

increased by 2- to 3-fold, while secondary inorganic ions (SO_4^{2-} and NO_3^-) showed smaller increases (1- to 3-fold), indicating active atmospheric aging (Peng et al., 2021). Notably, secondary inorganic ions and $PM_{2.5}$ during FII were lower than background levels (FII/BII < 1). The overall enhancements during FII were substantially smaller than those during FI, reflecting the brief duration of the Lantern Festival firework event rather than suppressed secondary formation. Therefore, the subsequent analysis focused primarily on FI, where the firework signals were most pronounced.

During the period when fireworks were permitted, air quality deteriorated sharply over a short timescale. Ba mass concentrations and Ba-containing particle counts exceeded background levels by approximately two orders of magnitude, with hourly peaks up to 1000-fold. This magnitude is comparable to that of severe firework events reported globally, such as Diwali celebrations in India (Kulshrestha et al., 2004; Tanda et al., 2019; Wang et al., 2007). These enhancements are substantially greater than the 4.5- to 40-fold increases documented in regions with stricter controls, consistent with findings by Huang et al. (2024).

Diurnal variations showed $PM_{2.5}$ mass concentration, Ba mass concentration, and Ba-containing particle counts rising sharply from evening, peaking at night (20:00–02:00) at levels more than an order of magnitude above background, then dropping rapidly in early morning (**Fig. 1b**). This pattern is directly linked to nighttime fireworks practices. Particle size analysis revealed significant increases in the 0.1–2.0 μm range (**Fig. 1c**). In the 0.5–1.0 μm fraction, Ba-containing particle counts surged from 2,193 during background to 24,624 during firework periods, underscoring the strong particle-generating capacity of fireworks in this size range. This pronounced increase in the 0.5–1.0 μm accumulation mode is consistent with previous findings that more than 80% of firework-generated metals, including Ba, are concentrated in the submicrometric region (<1 μm) (Crespo et al., 2012). A 6.7-fold increase in particle number concentration in the 0.5–1.0 μm range during Milan fireworks has been reported (Vecchi et al., 2008), which is lower than the 11.2-fold increase observed here, suggesting particularly intense firework emissions in this study.

3.1.2 Spatial heterogeneity across policy zones

The observed urban–rural gradient appears to be associated with regulatory measures and human activity intensity rather than simple downwind dispersion, and both $PM_{2.5}$ and Ba peak mass concentrations exhibited similar spatial patterns (**Fig. 2**). The highest concentration ($PM_{2.5}$: 89 μg m^{-3}; Ba: 3,411 ng m^{-3}) occurred at PYDXC, a restricted-fireworks suburban area with high population density (5,327 people km^{-2}; Guangzhou Statistical Yearbook, 2023). In contrast, the urban core site (GYQ), despite higher population density (28,400 people km^{-2}, 2023 data), exhibited lower peak concentrations. Concentrations at suburban NSPZ were slightly lower than the urban core, while the rural background site (CHLK) showed the lowest levels. This pattern suggests that regulatory policy (ban vs. restriction) is consistent with a possible influence on spatial heterogeneity of peak pollution during episodic events, although other factors such as local firework activity, enforcement intensity, meteorological conditions, atmospheric transport, and proximity to emission sources may also contribute (Kong et al., 2015). Thus, our

interpretation should be considered preliminary and warrants verification with additional data (e.g., enforcement records and wind field analysis).

3.2 Mixing state and identification of early-aged and more aged particle types

3.2.1 Mixing state and chemical characteristics of Ba-containing particles

Fig. 3a presents the mass spectra of two representative single particles, OClN and N, which exhibited the most distinct chemical fingerprints among the four categories identified in Section 2.3. These two types were selected to illustrate the contrasting chemical features between particles with different mixing states, while the average mass spectra of the remaining types (NS and S) are provided in **Fig. S3b**. The OClN particles are characterized by intense Ba^+ [*m/z* 138] and BaO^+ [*m/z* 156] signals in the positive ion spectrum, along with prominent Cl^- [*m/z* –35], O^- [*m/z* –16], and NO_3^- [*m/z* –62] peaks in the negative ion spectrum. In contrast, the N type particles exhibit a pronounced increase in the relative peak area of NO_3^- [m/z –62], while the Cl^- signal remains relatively unchanged. To quantify the distribution of these chemical types across the entire aerosol population, we examined the mixing states of all detected Ba-containing particles at the four sites during FI (**Fig. 3b**). The majority were internally mixed with nitrate (N type, 62.4%), followed by particles mixed with both chloride and nitrate (OClN type, 13.8%), and those containing sulfate (NS and S types combined, 13.6%). Particles with other mixing states accounted for the remaining 10.2%. The temporal evolution of these particle types further reveals the aging process (**Fig. 3c**). During the early phase of FI, OClN particles were more abundant with clear diurnal variations, while later periods saw increased proportions of aged types (N and NS). This shift provides additional evidence for progressive atmospheric aging of firework-derived aerosols.

3.2.2 Evidence for early-aged and more aged particle types and their physical mixing

Multiple lines of evidence suggest that OClN particles are relatively early-aged compared to N particles, which appear more nitrate-rich and processed. OClN particles are distinguished by enriched chloride (mean RPA of $^{35}Cl^-$ > 0.05, **Fig. S2**). Although barium chlorate [$Ba(ClO_3)_2$] is used as a green colorant, it decomposes above 250 °C and is unlikely to be emitted as such. The observed Cl^- enrichment, together with ubiquitous K^+[*m/z* 39] (**Fig. 3a**), indicates OClN particles exist as chlorides (e.g., $BaCl_2$) rather than chlorate. In contrast, N particles are dominated by nitrate (**Fig. 3a**), with the combined RPA of NO_3^- and NO_2^- accounting for about 70% of the total negative ion signal (**Fig. S2**). This nitrate dominance reflects atmospheric oxidative processing, consistent with previous studies (Xue et al., 2014; Zhang et al., 2015). During the transition from firework to post-firework hours, aging was evidenced by a decrease in both the number fraction of Cl-containing particles (from 24% to 21%) and the RPA of Cl^- (from 0.059 to 0.040), accompanied by an increase in nitrate RPA (from 0.355 to 0.415) (Huang et al., 2024).

Time series analysis revealed an inverse relationship between OClN and N particles during periods of intense emissions (r =

–0.709, p < 0.01; **Fig. S5a**), consistent with reported aging timescales of firework aerosols (Carrico et al., 2018; Reyes-Villegas et al., 2018). Size distributions show that N particles are preferentially found in smaller sizes compared to OClN (**Figs. S5b and S6**), consistent with the interpretation that chloride-to-nitrate conversion may be accompanied by an increase in particle density, as suggested in previous studies (Liu et al., 2017; Wang et al., 2013). Beyond chemical differences, aging also involves physical coagulation with Al- and Mg-containing particles. Al-Mg particles mixed preferentially with OClN (60–80%) over N particles (20–40%) throughout the study period (**Fig. S5c**). These single-particle observations complement bulk studies (Kong et al., 2015) by directly observing physical coagulation as an additional aging pathway alongside chemical transformation.

To further examine the spatial evolution of the aging process, we compared the OClN/N particle number ratios across the four sites during FI (**Fig. S7a**). The highest mean OClN/N particle number ratios were observed at NSPZ (**Fig. S7a**), particularly during nighttime hours (**Fig. S7b**), consistent with its proximity to active firework emission zones. At GYQ and CHLK, the OClN/N ratios were lower than at NSPZ, suggesting progressive aging of Ba-containing particles during atmospheric transport. Notably, PYDXC, despite being a restricted-firework zone with a moderate Ba-containing particle fraction (2.2%, **Table 1**) and the highest NO_2 enhancements among all sites (**Table 2**), exhibited unexpectedly low OClN/N ratios. This may reflect rapid aging driven by locally elevated NO_2 levels, which could accelerate chloride-to-nitrate conversion, or differences in firework composition and local chemical conditions compared to NSPZ. These site-specific patterns, together with the diurnal variations of OClN/N ratios at NSPZ (**Fig. S7b**), provide complementary evidence for the proposed aging pathway and highlight the role of local chemical environments in modulating the aging process. Wind-direction analysis also supported these site-specific patterns, with higher OClN/N ratios at PYDXC corresponding to the direction of restricted firework zones, and at NSPZ predominantly from the north and northwest, consistent with its geographical setting (**Fig. S8**). Backward trajectory analysis further showed that, at all four sites, OClN/N high values were predominantly associated with short-range air masses, suggesting local or nearby sources rather than long-range transport (**Fig. S9**).

It should be acknowledged that the classification of OClN and N particles as early-aged and more aged states is based on observed chemical evolution in ambient aerosols, rather than on direct near-source sampling of fresh firework emissions. Without such reference measurements, we cannot definitively characterize the initial emission state of Ba-containing particles. Nevertheless, the consistent temporal patterns support the interpretation that OClN particles represent a less advanced stage of aging compared to N particles.

3.3 Chemical transformation and aging mechanisms

3.3.1 Chemical transformation from chloride to nitrate

Synthesizing the evidence presented above, we propose that firework-derived Ba-containing particles undergo distinct aging pathways in the atmosphere. Fresh primary Ba-containing particles were not directly sampled; therefore, OClN and N are interpreted only as relatively early-aged and more-aged ambient states, respectively. The 9–10 hours lag between OClN and N

particle peaks (Δt_1), together with the 2–4 hours lag between gaseous NO_2 and particulate nitrate peaks (Δt_2) (**Fig. 4a**), points to nitrate formation as an important aging pathway.

This conversion proceeds through distinct chemical stages captured by the compositional characteristics of Ba-OClN and Ba-N particles, subsets of OClN and N that are rich in Ba with minimal interference from Al and Mg, enabling direct investigation of Ba-associated chemical transformations. In Ba-OClN representing a partially aged state, peak areas of chloride show a slight increase with peak areas of Ba, while nitrate signals decrease markedly (by approximately 43% from the lowest to the highest Ba interval) (**Fig. 5a**). The $Cl^-/(Cl^-+NO_3^-)$ ratio increases with Ba at lower intervals but exhibits a slight decrease at the highest Ba interval. This dominance of chloride across most Ba ranges, together with the inverse relationship between nitrate and particle mass, indicates that Ba-OClN particles are consistent with chloride-rich Ba-containing particles, with nitrate present as a minor component likely acquired during initial aging. The higher relative proportion of large peak areas in Ba-OClN particles (**Fig. S10**) further supports their less aged nature compared to Ba-N particles.

In contrast, Ba-N particles exhibit a distinctly different compositional pattern (**Fig. 5b**). Both chloride and nitrate peak areas increase with those of Ba, with nitrate showing a particularly strong increase at lower Ba levels followed by a clear plateau at higher Ba levels (Ba peak area > 10000). The $NO_3^-/(Cl^-+NO_3^-)$ ratio remains consistently above 0.9 across all Ba intervals. This nitrate-dominated composition, with chloride reduced to a minor residual component (<10%), indicates that Ba-N particles are consistent with nitrate-rich Ba-containing particles. The observed plateau in nitrate peak area with increasing Ba peak area suggests that nitrate incorporation into Ba-containing aerosols may be limited under the conditions of this study, reaching a point beyond which further uptake slows. This contrasts with the early-aged Ba-OClN particles, where nitrate remains a minor component and does not accumulate with increasing Ba peak area.

It should be noted, however, that fireworks contain nitrate-based oxidizers such as KNO_3 and $Ba(NO_3)_2$, which may directly emit primary nitrate-containing particles upon combustion (Conkling and Mocella, 2010; Wang et al., 2007). Therefore, the observed nitrate enrichment in Ba-containing particles cannot be solely attributed to secondary aging processes. Nevertheless, the diurnal variations of NO_3^-/K^+, NO_3^-/Ba, and Cl^-/NO_3^- mass concentration ratios are consistent with the proposed aging pathway (**Fig. S11**). The NO_3^-/K^+ ratio was consistently higher during daytime than during nighttime, consistent with greater relative nitrate abundance. Conversely, the Cl^-/NO_3^- ratio was significantly elevated during nighttime, reflecting the direct emission of chloride-rich particles from active fireworks. In contrast, the NO_3^-/Ba ratio remained relatively stable throughout the diurnal cycle, consistent with the relatively stable ratios observed in Ba-N particles (**Fig. 5b**). These patterns, together with the temporal lags between OClN and N particle peaks and between gaseous NO_2 and particulate NO_3^-, suggest that secondary nitrate formation via chloride-to-nitrate conversion is an important aging pathway, although primary nitrate emissions from fireworks may also contribute. In our dataset, we cannot fully quantify the relative contributions of these two sources. Future studies using high-time-resolution tracer analyses are needed to better distinguish them.

3.3.2 Possible aging mechanisms of Ba

Several mechanisms may contribute to the observed nitrate formation. The coexistence of O_3 and NO_2 at night is consistent with the N_2O_5 hydrolysis pathway, a common nighttime nitrate formation route (Brown et al., 2012; Zhao et al., 2023; Zhao et al., 2026). However, the moderate humidity (~60%, **Fig. S12**) during peak firework events suggests additional pathways may also be involved, such as heterogeneous uptake of HNO_3 on chlorine-rich particles (Liu et al., 2007; Vlasenko et al., 2006) or liquid-phase reactions mediated by hygroscopic salts (Cheng et al., 2016). The observed nitrate saturation in Ba-N particles likely reflects constraints on further nitrate uptake. Possible explanations include surface site limitation (Ravishankara et al., 1997), thermodynamic equilibrium with gas-phase HNO_3 (Guo et al., 2017), or phase transitions that limit internal diffusion (Koop et al., 2011). Distinguishing among these mechanisms will require further investigation using laboratory studies and thermodynamic modeling.

The aging pathways described above are further modulated by particle size, mixing state, and site-specific conditions. Notably, the $NO_3^-/(NO_3^-+Cl^-)$ ratio in Al-Mg-OClN particles decreases with increasing particle size, while in OClN particles without Al/Mg, this ratio shows little size dependence (**Fig. 4c**). This contrast suggests that the presence of Al and Mg may influence chloride-to-nitrate conversion efficiency (Li et al., 2023; Reinsch et al., 2010). Spatially, the extent of aging varies considerably among sites **(Figs. 4b and 4d)**: at PYDXC, the coexistence of early-aged and partially aged particles reflects active local emissions; at NSPZ, the higher abundance of aged N particles indicated more extensive aging during transport; at background sites, the dominance of fully processed, nitrate-saturated particles represents the terminal aging state under regional transport influences (Zhang et al., 2019; Zhang et al., 2022). This spatial gradient provides a complementary perspective to the temporal evolution captured at individual sites, confirming that chloride-to-nitrate conversion progresses continuously during atmospheric transport (Denkenberger et al., 2007). These chemical and physical processes are not independent; chemical transformation alters particle surface properties, facilitating further coagulation, which in turn provides fresh surfaces for additional heterogeneous reactions. This interplay ultimately governs the atmospheric lifetime and transport potential of firework-derived Ba aerosols.

3.4 Preliminary exposure and risk assessment

HQs for Ba were calculated for children and adults based on measured Ba mass concentrations (**Table 3**). HQ values ranged from 6.11E-08 to 2.77E-05 for children and from 3.44E-08 to 1.56E-05 for adults across all sites. All HQs were substantially below 1, indicating values below the threshold of concern under the screening-level assumptions, within the limitations of this assessment. Spatially, HQ followed the pattern of Ba mass concentrations, with the highest at PYDXC and the lowest at CHLK, consistent with the pattern of Ba mass concentrations and suggesting that particle concentration is a key determinant of health risk. Children exhibited higher HQ than adults due to their greater respiratory rate per unit body weight, highlighting the need to protect sensitive populations (Kong et al., 2012; Samoli et al., 2010). Temporally, HQ during FI was 1–2 orders of magnitude

higher than during background periods, consistent with observations from Shanghai (Liu et al., 2019). Although the long-term risk is acceptable, this short-term peak exposure may warrant further investigation for potential acute effects, particularly for individuals with respiratory conditions (Godri et al., 2012).

It should be noted that the HQ estimates presented here are based on period-specific average concentrations and are intended for relative comparison between firework-impacted and background periods, rather than as a definitive assessment of annual chronic risk.

Firework exposure is highly episodic, with Ba mass concentrations exhibiting sharp spikes lasting only a few hours during active firework periods (**Fig. 1a**). While the chronic HQ based on long-term average concentrations was below 1, the short-term peak concentrations during these episodes were 1–3 orders of magnitude higher than background levels. A formal acute HQ was not calculated due to the lack of an established acute reference value for Ba. Nevertheless, the elevated peak concentrations suggest that transient exposure events may pose a greater concern than the long-term average would indicate, particularly for children and individuals with pre-existing respiratory or cardiovascular conditions.

Several uncertainties should be considered in interpreting these results. First, the use of an oral RfD as a substitute for an inhalation reference concentration may not fully capture inhalation-specific bioavailability. Second, the health risk of Ba-containing particles may depend on their chemical speciation (e.g., $BaCl_2$ vs. $Ba(NO_3)_2$), solubility, and bioavailability, which were not directly measured in this study (ATSDR, 2021). These factors represent important uncertainties in this preliminary screening-level assessment and warrant further investigation. However, this interpretation is qualitative and does not imply a quantified acute health risk, as no formal acute HQ was calculated.

4. Conclusions and implications

This study provides direct single-particle evidence of rapid atmospheric aging and mixing-state evolution in firework-derived Ba aerosols within urban environments. During firework episodes, Ba mass concentrations were 1–3 orders of magnitude above background levels. Chloride-rich OClN and nitrate-dominated N particles were interpreted as relatively early and more advanced stages of atmospheric aging, respectively. Al/Mg mixing patterns and several-hour temporal lags provided complementary evidence for physical mixing during early aging and secondary nitrate formation. Site-level Ba contrasts were consistent with a potential mitigating influence of stricter controls. Primary nitrate emissions and site-specific emission and transport conditions may also have contributed to the observed patterns; nevertheless, the convergence of chemical, temporal, and spatial evidence provides mechanistic insights into the rapid atmospheric aging of firework-derived Ba particles and highlights the relevance of differentiated firework-control measures when interpreting spatial pollution contrasts.

These findings have several implications. First, the observed aging of firework-derived particles over several hours suggests that substantial secondary processing can occur within urban airsheds, potentially influencing local air quality before regional transport. Second, the observed shift toward smaller particle sizes upon chloride-to-nitrate conversion may enhance respiratory deposition potential. Third, the preferential association of Al-Mg with early-aged particle populations suggests that coagulation

is most active during early aging stages, potentially altering particle hygroscopicity and reactivity. Fourth, although all screening-level HQ estimates based on an oral RfD surrogate were below 1, peak Ba concentrations during firework events were 1–3 orders of magnitude above background levels, warranting further assessment of their potential inhalation-related health implications. Single-particle analysis provides a framework for investigating aging mechanisms of other metal-containing particles emitted by fireworks. When combined with bulk mass concentration measurements, records of firework activity and enforcement, and meteorological data, it may also support future assessments of emission-control measures. Future studies should combine near-source sampling with high-time-resolution tracer measurements to distinguish primary nitrate emissions from secondary nitrate formation. They should also characterize changes in Ba speciation, solubility, and bioavailability during atmospheric aging and determine whether similar processes occur in other metal-containing particles emitted by fireworks.

Supplement. Supporting information includes twelve figures (Fig. S1–S12) related to the manuscript.

Data availability. The observational data including SPAMS and meteorological parameters used in this study are available from corresponding authors upon request (limei@jnu.edu.cn).

Author contributions. ML designed the research with input from CP, XB, GZ, and ZZ. WS, CL, LL and KH collected samples. XL processed data and wrote the manuscript. BH, and CC had an active role in supporting the writing-original work. All authors contributed to the discussions of the results and refinement of the manuscript.

Competing interests. The authors declare that they have no conflict of interest.

Financial support. This work was supported by the National Natural Science Foundation of China (grant no. 42407355).

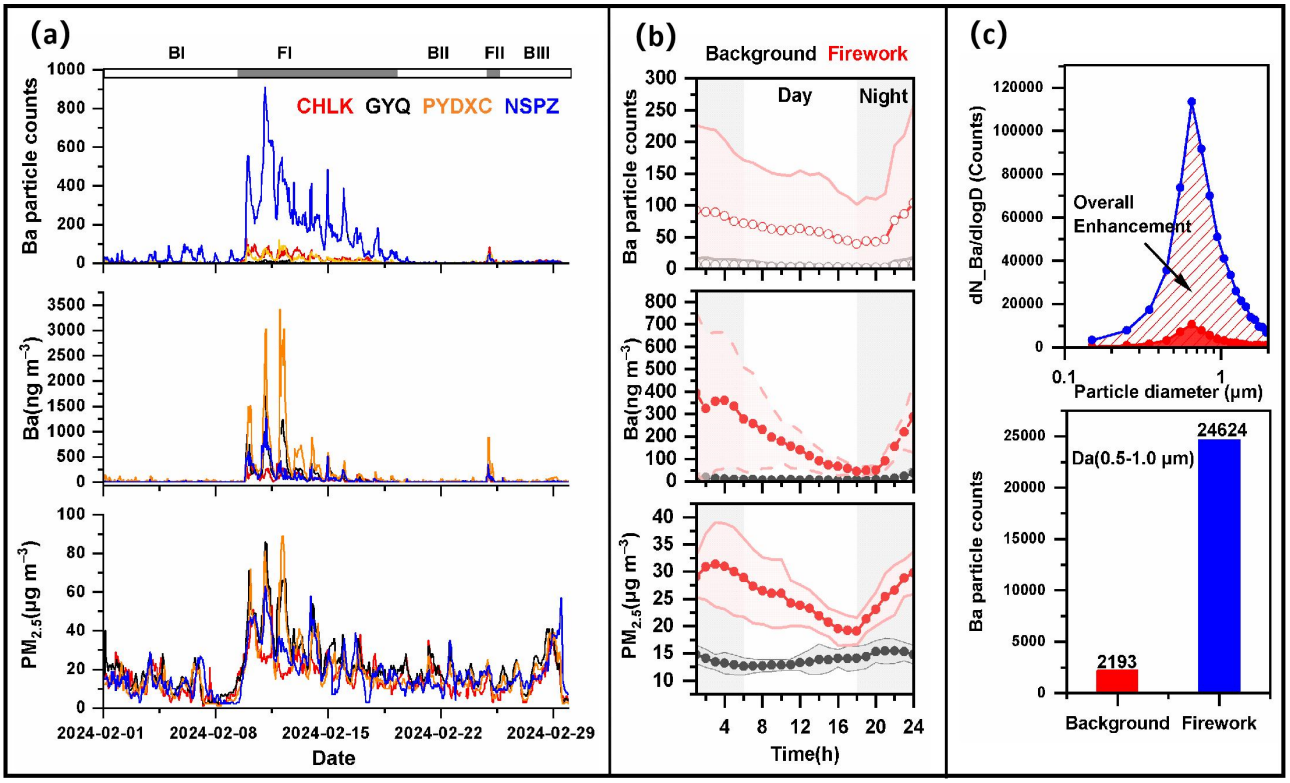

Figure 1. Temporal variations and size distributions of particulate matter. (a) Time series of $PM_{2.5}$ mass concentration, Ba mass concentration, and Ba-containing particle counts at the four sites (firework periods shaded), respectively. (b) Diurnal patterns of $PM_{2.5}$ mass concentration, Ba mass concentration and Ba-containing particle counts at the four sites during firework periods (red) and background periods (black). (c) Upper panel: particle size distributions of Ba-containing particles (plotted as dN_Ba/dlogD); lower panel: comparison of total Ba-containing particle counts in the 0.5–1.0 μm size range between background and firework periods.

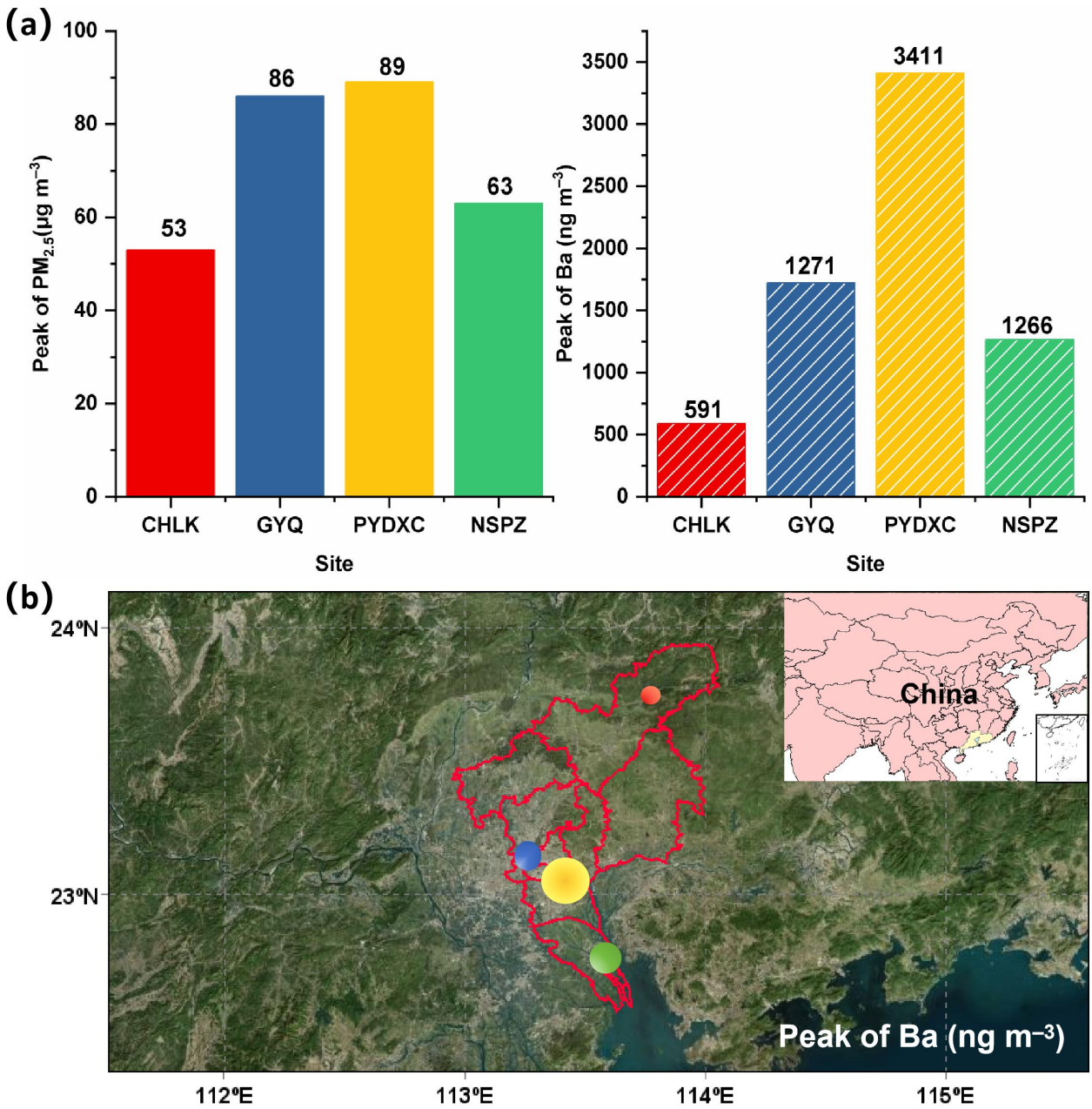

Figure 2. Spatial heterogeneity of firework-derived particulate matter pollution. (a) Peak $PM_{2.5}$ and Ba mass concentrations at the four sites, respectively. (b) Map of the study area, where the bubble size represents the peak Ba mass concentration at each site. Basemap: Bing Satellite, processed with MeteoInfo. © Microsoft.

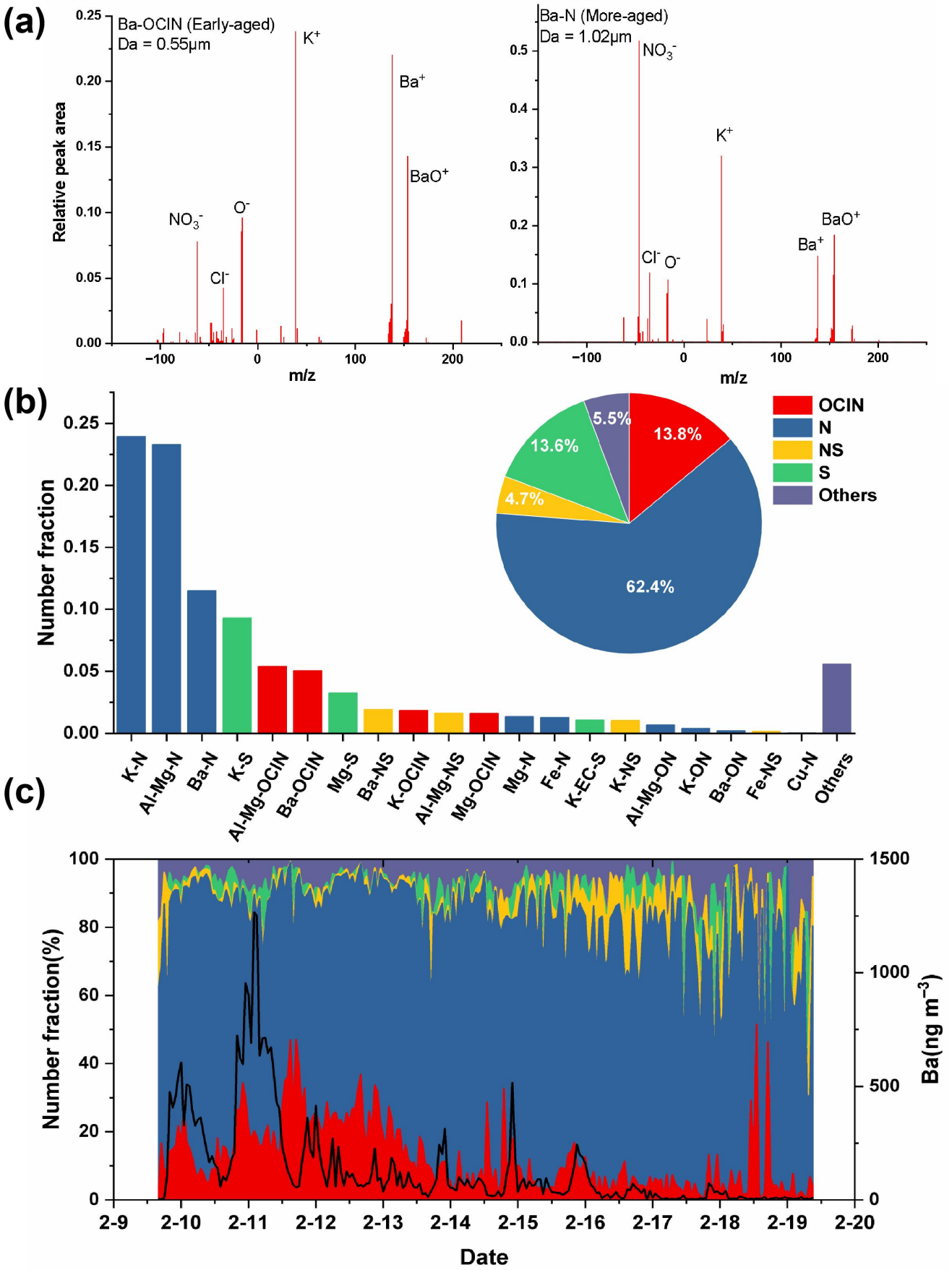

Figure 3. Chemical characteristics of Ba-containing particles during FI. (a) Mass spectra of early-aged (Ba-OClN) and more aged (Ba-N) particle types. (b) Average abundances of the 21 particle subtypes at the four sites (bar chart) and their reclassified fractional composition into four major groups (OClN, N, NS, S) (pie chart). (c) Temporal variations of the four main particle types (stacked bars, left axis) and Ba mass concentration (line, right axis) at the four sites.

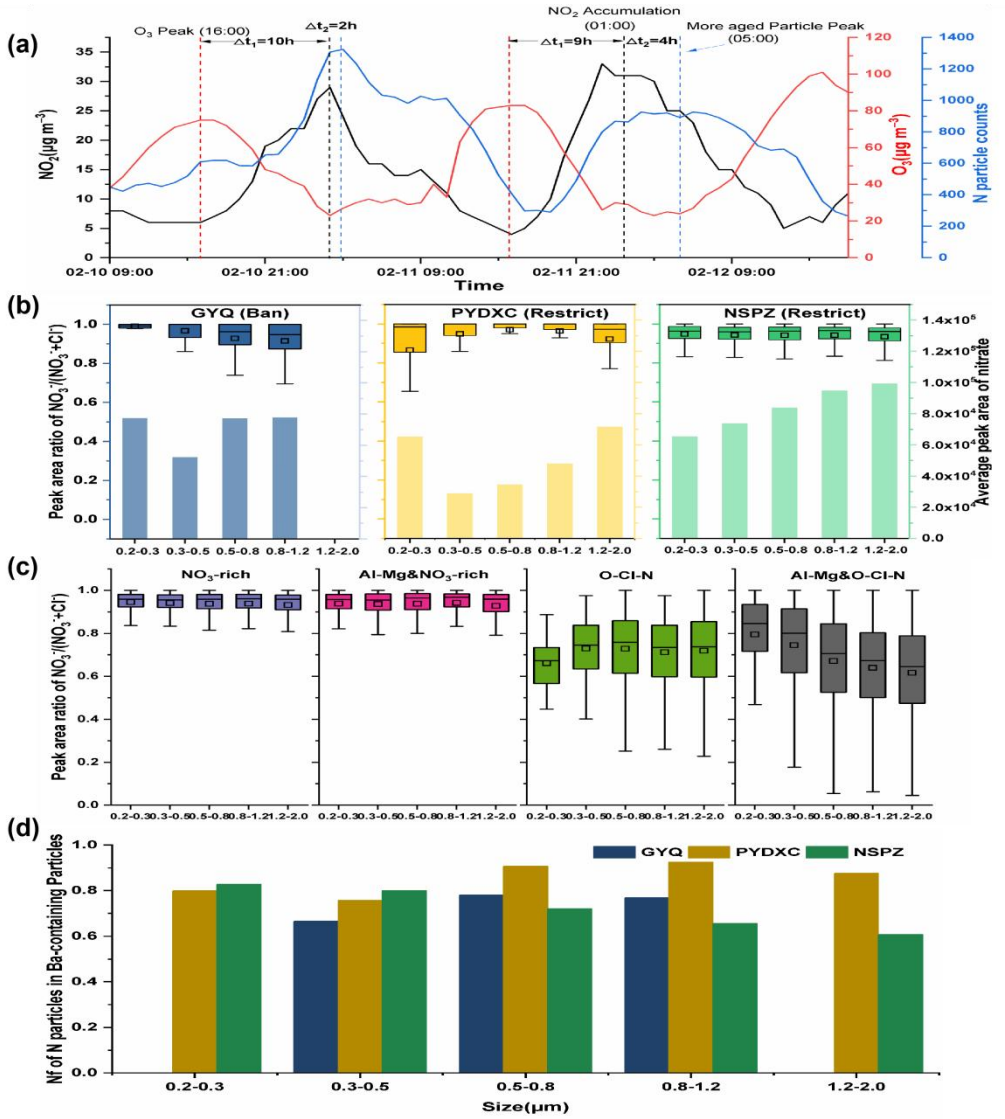

Figure 4. Nighttime aging and size-dependent nitrate formation during FI. (a) Time series of O_3, NO_2, and N particles counts (weighted regional averages from GYQ, PYDXC, and NSPZ) during two high-intensity firework days. (b) $NO_3^-/(NO_3^-+Cl^-)$ ratio (left) and mean nitrate peak area (right) by particle size at restricted (PYDXC, NSPZ) and prohibited sites (GYQ). (c) $NO_3^-/(NO_3^-+Cl^-)$ ratio by particle size at NSPZ. (d) Number fraction(Nf) of N particles among Ba-containing particles by particle size at GYQ, PYDXC, and NSPZ, respectively.

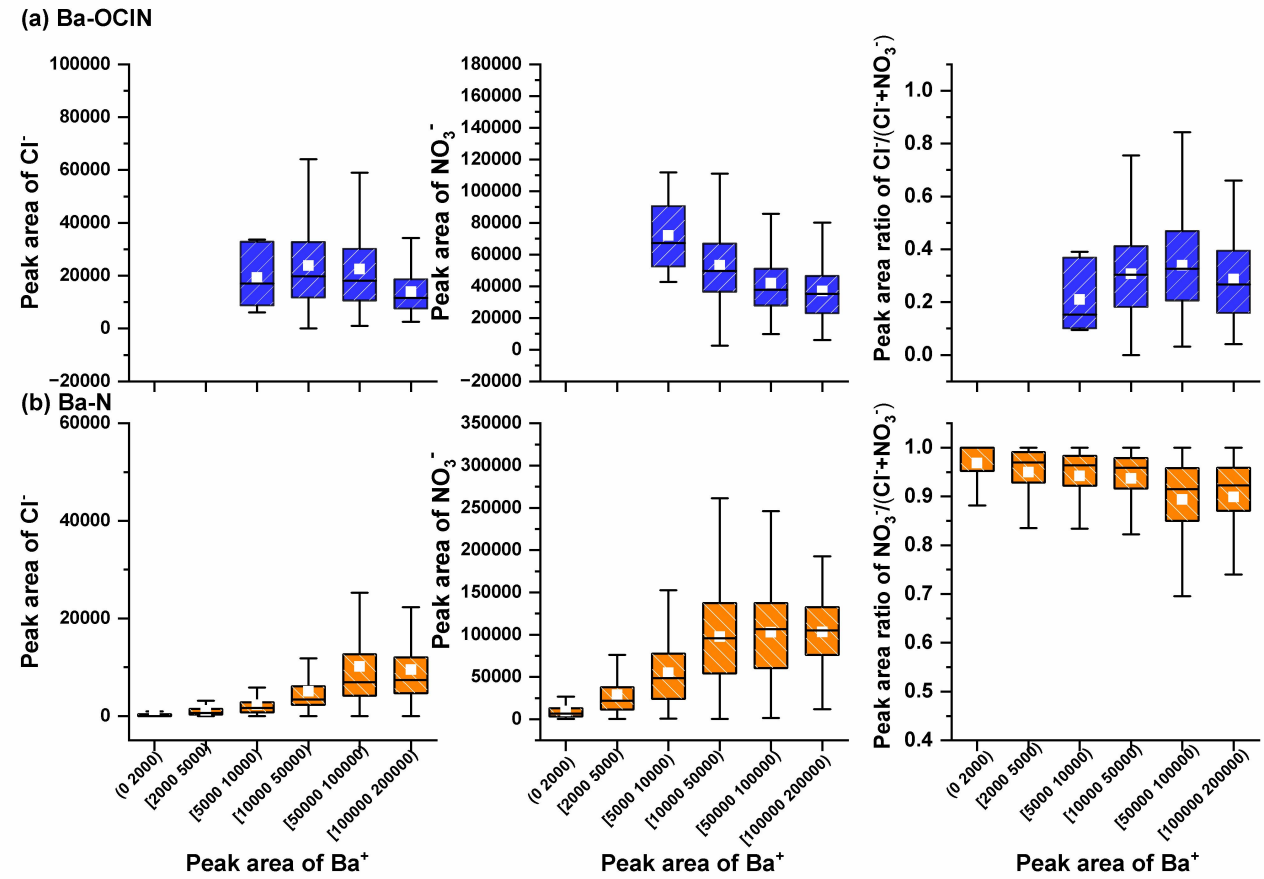

Figure 5. Box plots of Cl^- peak area, NO_3^- peak area, and (a) $Cl^-/(Cl^-+NO_3^-)$ or (b) $NO_3^-/(Cl^-+NO_3^-)$ ratio across Ba peak area bins for Ba-OClN and Ba-N particles, respectively, at the NSPZ site during FI.

Table 1 A summary of the dates of the SPAMS measurements and the number and number fraction (Nf) of the detected Ba-containing particles over the entire sampling period.

	CHLK		GYQ		PYDXC		NSPZ	
Species	Number	Nf(%)	Number	Nf(%)	Number	Nf(%)	Number	Nf(%)
All particles [a]	585933		71392		332888		1347245	
Ba-containing	8422	1.4% [b]	679	1.0%	6733	2.0%	59010	4.4%
Al-Mg-N	1396	16.6% [c]	128	18.9%	2821	41.9%	10197	17.3%
Al-Mg-OClN	802	9.5%			34	0.5%	5568	9.4%
Al-Mg-ON			33	4.9%			1727	2.9%
Al-Mg-NS	42	0.5%					407	0.7%
Ba-N	958	11.4%	111	16.3%	1345	20.0%	6732	11.4%
Ba-OClN	31	0.4%	42	6.2%			1276	2.2%
Ba-ON							518	0.9%
Ba-NS	48	0.6%					153	0.3%
K-N	2895	34.4%	247	36.4%	1601	23.8%	19713	33.4%
K-ON							901	1.5%
K-OClN	216	2.6%	79	11.6%	136	2.0%	1160	2.0%
K-NS	645	7.7%	16	2.4%			156	0.3%
K-S			11	1.6%				
K-EC-S	142	1.7%						
Mg-N	221	2.6%					1590	2.7%
Mg-OClN							3465	5.9%
Mg-S	51	0.6%						
Cu-N							112	0.2%
Fe-N	122	1.4%			364	5.4%	823	1.4%
Fe-NS	29	0.3%					108	0.2%
Others	824	9.7%	12	1.7%	432	6.4%	4404	7.3%

[a]All particles were detected with both positive and negative spectra. [b]Nf was calculated through the number of Ba-containing particles by the number of all particles over the sampling period. [c]Nf was calculated through the number of clustered Ba-containing particles by Ba-containing particles over the sampling period.

Table 2 The average values and standard deviations of $PM_{2.5}$, meteorological parameters, and the main water-soluble inorganic ions and heavy metals related to firework emissions at the four sites during different pollution periods.

Parameter (Unit)	Site	BI	FI	BII	FII	BIII	FI/BI (Fold)	FII/BII (Fold)
		Mean ± SD						
$PM_{2.5}$ (μg m^{-3})	CHLK	11.2 ± 6.7	21.6 ± 8.0	13.7 ± 5.9	7.9 ± 5.3	14.5 ± 9.6	1.9	0.6
	GYQ	13.3 ± 6.7	32.2 ± 15.4	18.1 ± 4.8	11.9 ± 2.8	19.4 ± 10.4	2.4	0.7
	PYDXC	10.0 ± 5.6	27.7 ± 16.9	14.0 ± 3.9	10.4 ± 4.7	17.5 ± 10.3	2.8	0.7
	NSPZ	11.0 ± 6.2	25.6±12.1	14.1 ± 5.1	12.2 ± 4.6	18.8 ± 10.8	2.3	0.9
Ba (ng m^{-3})	CHLK	2.5 ± 2.0	84.6 ± 91.8	4.2 ± 17.1	25.7 ± 60.2	2.2 ± 1.3	33.8	6.1
	GYQ	4.5 ± 6.6	185.6 ± 274.6	9.4 ± 33.8	30.1 ± 36.4	4.7 ± 7.6	40.9	3.2
	PYDXC	23.0 ± 25.2	398.5 ± 623.5	25.1 ± 80.0	144.1 ± 226.4	27.0 ± 26.3	17.3	5.8
	NSPZ	4.8 ± 6.2	137.5±207.4	8.9±35.1	42.3 ± 53.2	7.6 ± 11.4	28.9	4.8
K^+ (μg m^{-3})	CHLK	0.1 ± 0.1	1.3 ± 1.0	0.2 ± 0.1	0.5 ± 0.5	0.2 ± 0.1	9.4	3.1
	GYQ	0.1 ± 0.1	1.6 ± 2.3	0.1 ± 0.1	0.2 ± 0.2	0.1 ± 0.1	23.2	1.5
	PYDXC	0.2 ± 0.1	2.5 ± 2.9	0.2 ± 0.2	0.9 ± 0.9	0.3 ± 0.1	14.6	4.5
	NSPZ	0.2 ± 0.1	1.9 ± 2.2	0.2 ± 0.2	1.0 ± 0.9	0.4 ± 0.2	11.2	4.7
Cl^- (μg m^{-3})	CHLK	0.07 ± 0.03	0.11 ± 0.03	0.09 ± 0.03	0.07 ± 0.02	0.10 ± 0.05	1.5	0.8
	GYQ	0.3 ± 0.3	0.7 ± 1.2	0.2 ± 0.1	0.2 ± 0.1	0.4 ± 0.4	2.6	0.9
	PYDXC	0.3 ± 0.3	1.0 ± 1.5	0.3 ± 0.2	0.5 ± 0.6	0.4 ± 0.5	3.0	1.9
	NSPZ	0.4 ± 0.3	0.9 ± 1.0	0.3±0.2	0.7 ± 0.5	0.7 ± 0.6	2.3	2.2
Cu (ng m^{-3})	CHLK	1.7 ± 2.0	25.7 ± 23.8	1.8 ± 4.1	7.0 ± 12.3	2.1 ± 2.0	14.7	3.9
	GYQ	4.3 ± 3.2	53.8 ± 72.2	5.0 ± 8.6	10.2 ± 8.2	5.9 ± 4.7	12.5	2.0
	PYDXC	117.2 ± 59.5	197.4 ± 209.7	59.9 ± 28.1	100.5 ± 66.8	61.8 ± 12.6	1.7	1.7
	NSPZ	4.1 ± 4.4	48.8 ± 66.4	8.6 ± 15.6	31.3 ± 31.5	12.1 ± 8.4	11.9	3.6
Pb (ng m^{-3})	CHLK	3.2 ± 5.8	5.8 ± 4.9	1.4 ± 3.8	1.0 ± 1.2	13.9 ± 31.9	1.8	0.7
	GYQ	4.1 ± 3.5	11.6 ± 12.1	4.8 ± 4.6	9.3 ± 2.8	10.3 ± 6.0	2.8	1.9
	PYDXC	10.5 ± 6.5	32.8 ± 34.5	9.2 ± 7.4	15.9 ± 12.2	16.1 ± 10.8	3.1	1.7
	NSPZ	2.0 ± 2.4	7.4 ± 8.2	4.1 ± 21.4	4.6 ± 2.6	6.9 ± 5.1	3.7	1.1
SO_4^{2-} (μg m^{-3})	CHLK	1.0 ± 0.8	1.4 ± 1.1	0.8 ± 0.4	0.9 ± 0.5	1.4 ± 1.0	1.5	1.1
	GYQ	3.4 ± 2.3	4.0 ± 1.8	2.5 ± 0.6	2.6 ± 0.5	3.7 ± 2.3	1.2	1.0
	PYDXC	2.8 ± 2.2	3.6 ± 1.5	1.9 ± 0.7	1.7 ± 0.5	3.2 ± 2.3	1.3	0.9
	NSPZ	3.2 ± 2.2	4.3 ± 2.6	2.1 ± 1.2	2.1 ± 0.5	4.3 ± 3.4	1.3	1.0
NO_3^- (μg m^{-3})	CHLK	1.6 ± 1.2	4.2 ± 1.6	4.0 ± 3.5	1.4 ± 1.0	2.0 ± 1.8	2.6	0.4
	GYQ	2.0 ± 1.0	4.8 ± 1.5	4.6 ± 2.3	3.1 ± 1.0	3.4 ± 1.9	2.4	0.7

	PYDXC	1.9 ± 1.0	5.1 ± 2.2	3.8 ± 1.8	2.3 ± 1.6	2.7 ± 1.7	2.7	0.6
	NSPZ	1.9 ± 0.9	5.0 ± 2.0	4.0 ± 2.4	3.7 ± 0.9	3.0 ± 1.9	2.6	0.9
	CHLK	6.4 ± 3.5	3.2 ± 1.1	5.2 ± 1.7	4.4 ± 0.7	6.6 ± 2.6	0.5	0.9
	GYQ	27.0 ± 12.2	23.4 ± 12.9	19.8 ± 5.2	18.1 ± 3.1	27.3 ± 6.9	0.9	0.9
SO_2 (μg m^{-3})	PYDXC	24.0 ± 14.0	13.9 ± 7.9	17.1 ± 6.6	13.4 ± 3.9	26.1 ± 10.2	0.6	0.8
	NSPZ	28.4 ± 16.8	17.0 ± 9.2	23.6 ± 11.3	16.7 ± 4.5	30.9 ± 12.4	0.6	0.7
	CHLK	5.7 ± 0.6	5.6 ± 0.7	6.1 ± 0.5	5.3 ± 0.6	5.6 ± 0.7	1.0	0.9
	GYQ	4.1 ± 0.4	5.5 ± 0.9	5.0 ± 0.5	4.1 ± 0.3	4.6 ± 0.5	1.3	0.8
NO_2 (μg m^{-3})	PYDXC	5.4 ± 1.4	8.7 ± 1.8	4.1 ± 1.2	5.9 ± 0.3	6.3 ± 0.5	1.6	1.5
	NSPZ	4.3 ± 1.0	5.1 ± 1.1	4.8 ± 1.0	4.2 ± 0.4	5.4 ± 1.1	1.2	0.9

CHLK: Conghua Liangkou (background site); GYQ: Gongyuanqian (urban prohibited zone); PYDXC: Panyu University City (restricted zone); NSPZ: Nansha Puzhou (restricted zone). The fold change (F/B) is calculated as the ratio of the average concentration during a fireworks episode to that in the preceding background period.

Table 3 The hazard quotients (HQs) for the four sites during different pollution periods.

Type	Site	HQ				
		BI	FI	BII	FII	BIII
Children	CHLK	1.56E-07	5.87E-06	1.46E-07	1.78E-07	6.11E-08
	GYQ	2.81E-07	1.29E-05	3.26E-07	2.09E-07	1.30E-07
	PYDXC	1.44E-06	2.77E-05	8.71E-07	1.00E-06	7.50E-07
	NSPZ	3.00E-07	9.54E-06	3.09E-07	2.94E-07	2.11E-07
Adult	CHLK	8.81E-08	3.31E-06	8.22E-08	1.01E-07	3.44E-08
	GYQ	1.59E-07	7.26E-06	1.84E-07	1.18E-07	7.36E-08
	PYDXC	8.10E-07	1.56E-05	4.91E-07	5.64E-07	4.23E-07
	NSPZ	1.69E-07	5.38E-06	1.74E-07	1.66E-07	1.19E-07

References

Agency for Toxic Substances and Disease Registry (ATSDR).: Toxicological Profile for Barium and Barium Compounds; U.S. Department of Health and Human Services, Public Health Service: Atlanta, GA. https://www.atsdr.cdc.gov/toxprofiles/tp24.pdf, 2021.

Brown, S. S., and Stutz, J.: Nighttime Radical Observations and Chemistry. Chem. Soc. Rev. 41, 6405-6447, https://doi.org/10.1039/c2cs35181a, 2012.

Carrico, C. M., Gomez, S. L., Dubey, M. K., and Aiken, A. C.: Low Hygroscopicity of Ambient Fresh Carbonaceous Aerosols from Pyrotechnics Smoke. Atmos. Environ. 178, 101-108, https://doi.org/10.1016/j.atmosenv.2018.01.024, 2018.

Cheng, Y., Zheng, G., and Wei, C.: Reactive Nitrogen Chemistry in Aerosol Water as a Source of Sulfate during Haze Events in China. Sci. Adv. 2, e1601530, https://doi.org/10.1126/sciadv.1601530, 2016.

Conkling, J. A. and Mocella, C.: Chemistry of Pyrotechnics: Basic Principles and Theory, 2nd ed., CRC Press, Boca Raton, FL, 2010.

Crespo, J., Yubero, E., Nicolás, J. F., Lucarelli, F., Nava, S., Chiari, M., and Calzolai, G.: High-Time Resolution and Size-Segregated Elemental Composition in High-Intensity Pyrotechnic Exposures. J. Hazard. Mater. 241-242, 82-91, https://doi.org/10.1016/j.jhazmat.2012.09.017, 2012.

Deepthiraju, B., and Varma, P.: Barium Toxicity - A Rare Presentation of Fireworks Ingestion. Indian Pediatr. 49, 762-762, https://doi.org/10.1007/s13312-012-0144-z, 2012

Denkenberger, K. A., Moffet R. C., and Holecek J. C.: Real-Time, Single-Particle Measurements of Oligomers in Aged Ambient Aerosol Particles. Environ. Sci. Technol. 41, 5439-5446, https://doi.org/10.1021/es070329l, 2007.

Godri, K. J., Green, D. C., Fuller, G. W., Dall'Osto, M., Beddows, D. C., Kelly, F. J., Harrison, R., and Mudway, I.: Particulate Oxidative Burden Associated with Firework Activity. Environ. Sci. Technol. 44, 8295-8301, https://doi.org/10.1021/es1016284, 2010.

Guo, H., Liu, J., and Froyd, K. D.: Fine Particle pH and Gas-Particle Partitioning of Inorganic Species in Pasadena, California, during the 2010 CalNex Campaign. Atmos. Chem. Phys. 17, 5703-5719, https://doi.org/10.5194/acp-2016-1158, 2017.

Healy, R. M., Sciare, J., Poulain, L., Crippa, M., Wiedensohler, A., Prev ̀ ôt, A. S. H., Baltensperger, U., Sarda-Estev ̀ e, R., McGuire, M. L., Jeong, C. H., McGillicuddy, E., O'Connor, I. P., Sodeau, J. R., Evans, G. J., and Wenger, J. C.: Quantitative determination of carbonaceous particle mixing state in Paris using single-particle mass spectrometer and aerosol mass spectrometer measurements. Atmos. Chem. Phys. 13 (18), 9479−9496, https://doi.org/10.5194/acp-13-9479-2013, 2013.

Guangzhou Municipal People's Government. Guangzhou Fireworks and Firecrackers Safety Management Regulation. https://gzpc.gov.cn/zlk/flfgwjk/gzrdflfg/dfxfg/jk/content/post_232539.html (accessed February 11, 2026).

Hu, U., Sun, Y., Yang, G., Liu, M., Gao, Y., Lin, L., Cao, Y., Liu, W., and Huo, Y., Liu, J.: Spring Festival Firework Activities Exacerbate Toxic Effects of Aerosol Essential Components. J. Hazard. Mater. 490, 137874, https://doi.org/10.1016/j.jhazmat.2025.137874, 2025.

Huang, X., Ge, Y., Yang, T., Song, Z., Yu, S., Li, Q., Wang, X., Wang, Y., Wang, X., and Su, J.: Relaxation of Spring Festival Firework Regulations Leads to a Deterioration in Air Quality. Environ. Sci. Technol. 58, 10185-10194, https://doi.org/10.1021/acs.est.4c00920, 2024.

Inomata, Y., Igarashi, Y., Chiba, M., Shinoda, Y., and Takahashi, H.: Dry and Wet Deposition of Water-Insoluble Dust and Water-Soluble Chemical Species during Spring 2007 in Tsukuba, Japan. Atmos. Environ. 43, 4503-4512, https://doi.org/10.1016/j.atmosenv.2009.06.048, 2009.

Kaur, A., and Parkash, C.: Barium: Presence in Environment and Health Effects. Ecol. Environ. Conserv. 28, 2210-2213,

https://doi.org/10.53550/eec.2022.v28i04.085, 2022.

Kong, S., Lu, B., Ji, Y., Zhao, X., Bai, Z., Xu, Y., Liu, Y., and Jiang, H.: Risk Assessment of Heavy Metals in Road and Soil Dusts within $PM_{2.5}$, PM_{10} and PM100 Fractions in Dongying City, Shandong Province, China. J. Environ. Monit. 14, 791-803, https://doi.org/10.1039/C1EM10555H, 2012.

Kong, S. F., Li, L., Li, X. X., Yin, Y., Chen, K., Liu, D. T., Yuan, L., Zhang, Y. J., Shan, Y. P., and Ji, Y. Q. The Impacts of Firework Burning at the Chinese Spring Festival on Air Quality: Insights of Tracers, Source Evolution and Aging Processes. Atmos. Chem. Phys. 15, 2167-2184, https://doi.org/10.5194/acp-15-2167-2015, 2015.

Koop, T., Bookhold, J., and Shiraiwa, M.: Glass Transition and Phase State of Organic Compounds: Dependency on Molecular Properties and Implications for Secondary Organic Aerosols in the Atmosphere. Phys. Chem. Chem. Phys. 13, 19238-19255, https://doi.org/10.1039/c1cp22617g, 2011.

Kulshrestha, U. C., Nageswara Rao, T., Azhaguvel, S., and Kulshrestha, M.: Emissions and Accumulation of Metals in the Atmosphere Due to Crackers and Sparkles during Diwali Festival in India. Atmos. Environ.38, 4421-4425, https://doi.org/10.1016/j.atmosenv.2004.05.044, 2004.

Lee, E. S., Sahay, K., O'Neil, E., Biswas, S., Dzhema, I., Huang, S.-M., Lin, P., Chang, M.-C. O., and Huai, T.: Tracer-Gas-Integrated Measurements of Brake-Wear Particulate Matter Emissions from Heavy-Duty Vehicles. Environ. Sci. Technol. 57, 15968-15978, https://doi.org/10.1021/acs.est.3c03673, 2023.

Li, W., Shi, Z., Yan, C., Yang, L., Dong, C., and Wang, W.: Individual Metal-Bearing Particles in a Regional Haze Caused by Firecracker and Firework Emissions. Sci. Total Environ. 443, 464-469, https://doi.org/10.1016/j.scitotenv.2012.10.109, 2013.

Li, L., Huang, Z., Dong, J., Li, M., Gao, W., Nian, H., Fu, Z., Zhang, G., Bi, X., and Cheng, P.: Real Time Bipolar Time-of-Flight Mass Spectrometer for Analyzing Single Aerosol Particles. Int. J. Mass Spectrom. 303, 118-124, https://doi.org/j.ijms.2011.01.017, 2011.

Li, Y., Zhou, Y., and Guo, W.: Molecular Imaging Reveals Two Distinct Mixing States of $PM_{2.5}$ Particles Sampled in a Typical Beijing Winter Pollution Case. Environ. Sci. Technol. 57, 10236-10245, https://doi.org/10.1021/acs.est.2c08694, 2023.

Lian, X., Zhang, G., Yang, Y., Lin, Q., Fu, Y., Jiang, F., Peng, L., Hu, X., Chen, D., Wang, X., Peng, P.A., Sheng, G., and Bi, X.H.: Evidence for the formation of imidazole from carbonyls and reduced nitrogen species at the individual particle level in the ambient atmosphere. Environ. Sci. Technol. Lett. 8, 9–15, https://doi.org/10.1021/acs.estlett.0c00722, 2021.

Liu, D., Whitehead, J., Alfarra, M. R., Reyes-Villegas, E., Spracklen, D. V., Reddington, C. L., Kong, S., Williams, P. I., Ting, Y. C., and Haslett, S.: Black-Carbon Absorption Enhancement in the Atmosphere Determined by Particle Mixing State. Nat. Geosci.10, 184-188, https://doi.org/10.1038/ngeo2901, 2017.

Liu, J., Chen, Y., Chao, S., Cao, H., Zhang, A., 2019. Levels and Health Risks of $PM_{2.5}$-Bound Toxic Metals from Firework/Firecracker Burning during Festival Periods in Response to Management Strategies. Ecotoxicol. Environ. Saf. 171, 406-413, https://doi.org/10.1016/j.ecoenv.2018.12.104, 2019.

Liu, Y., Cain, J. P., Wang, H., and Laskin, A.: Kinetic Study of Heterogeneous Reaction of Deliquesced NaCl Particles with Gaseous HNO_3 Using Particle-on-Substrate Stagnation Flow Reactor Approach. Environ. Sci. Technol. 41, 6497-6502, https://doi.org/10.1021/jp072005p, 2007.

Peng, J., Hu, M., Shang, D., Wu, Z., Du, Z., Tan, T., Wang, Y., Zhang, F., and Zhang, R.: Explosive Secondary Aerosol Formation during Severe Haze in the North China Plain. Environ. Sci. Technol. 55, 2189-2207, https://doi.org/10.1021/acs.est.0c07204, 2021.

Ravishankara, A. R.: Heterogeneous and Multiphase Chemistry in the Troposphere. Science 1997, 276, 1058-1065, https://doi.org/10.1126/science.276.5315.1058, 1997.

Reinsch, B. C., Forsberg, B. , and Penn, R. L.: Chemical Transformations during Aging of Zerovalent Iron Nanoparticles in the Presence of Common Groundwater Dissolved Constituents. Environ. Sci. Technol. 44, 3455-3461,

https://doi.org/10.1021/es902924h, 2010.

Reyes-Villegas, E., Priestley, M., Ting, Y. C., Haslett, S., Bannan, T., Le Breton, M., Williams, P. I., Bacak, A., Flynn, M. J., and Coe, H.: Simultaneous Aerosol Mass Spectrometry and Chemical Ionisation Mass Spectrometry Measurements during a Biomass Burning Event in the UK: Insights into Nitrate Chemistry. Atmos. Chem. Phys. 18, 4093-4111, https://doi.org/10.5194/acp-2017-60510.5194, 2018.

Salma, I., Farkas, Á., and Weidinger, T.: Balogh, M. Firework Smoke: Impacts on Urban Air Quality and Deposition in the Human Respiratory System. Environ. Pollut. 328, 121612, https://doi.org/10.1016/j.envpol. 2023.121612, 2023.

Samoli, E., Nastos, P., Paliatsos, A., Katsouyanni, K., and Priftis, K.: Acute Effects of Air Pollution on Paediatric Asthma Exacerbation: Evidence of Association and Effect Modification. Eur. Respir. J. 36 (Suppl. 54), 523s, https://doi.org/10.7490/F1000RESEARCH.523.1, 2010.

Sharma, R., and Thakur, S.: Chapter 36-Barium Sulfate: Human Effects Assessment and Toxicological Profile. In Hazardous Chemicals, Chawla, M., Singh, J., Kaushik, R. D., Eds., Academic Press, pp 517-531, 2025.

Song, X. H., Hopke, P. K., Fergenson, D. P., and Prather, K. A.: Classification of Single Particles Analyzed by ATOFMS Using an Artificial Neural Network, ART-2A. Anal. Chem. 71, 860-865, https://doi.org/10.1021/ac9809682, 1999.

Tanda, S., Libinsk, R., Hegrová, J., and Goessler, W.: Impact of New Year's Eve Fireworks on the Size Resolved Element Distributions in Airborne Particles. Environ. Int. 128, 371-378, https://doi.org/10.1016/j.envint.2019.04.071, 2019.

Twohy, C., and Doran, C.: Field Performance Evaluation of the Cooper Environmental Services Ambient Metals Monitor (Xact 620) for Near-Real Time PM_{10} Metals Monitoring, Cooper Environmental Services. http://aaarabstracts.com/2010/viewabstract.php?id=788, 2010.

Vecchi, R., Bernardoni, V., Cricchio, D., D'Alessandro, A., Fermo, P., Lucarelli, F., Nava, S., Piazzalunga, A., and Valli, G.: The Impact of Fireworks on Airborne Particles. Atmos. Environ. 42, 1121-1132, https://doi.org/10.1016/j.atmosenv.2007.10.047, 2008.

Vlasenko, A., Sjogren, S., and Weingartner, E.: Effect of Humidity on Nitric Acid Uptake to Mineral Dust Aerosol Particles. Atmos. Chem. Phys. 6, 2147-2160, https://doi.org/10.5194/acp-6-2147-2006, 2006.

Wang, G. H., Zhou, B. H., Cheng, C. L., Cao, J. J., Li, J. J., Meng, J. J., Tao, J., Zhang, R. J., and Fu, P. Q.: Impact of Gobi Desert Dust on Aerosol Chemistry of Xi'an, Inland China during Spring 2009: Differences in Composition and Size Distribution between the Urban Ground Surface and the Mountain Atmosphere. Atmos. Chem. Phys. 13, 819-835, https://doi.org/10.5194/acp-13-819-2013, 2013.

Wang, W., Zhou, H., Gao, Y., Shao, L., Zhou, X., Li, X., Wei, D., Xing, J., and Lyu, R.: Chemical Composition and Morphology of $PM_{2.5}$ in a Rural Valley during Chinese New Year's Eve: Impact of Firework/Firecracker Display. Atmos. Environ. 318, 120225, https://doi.org/10.1016/j.atmosres.2016.07.028, 2024.

Wang, Y., Zhuang, G., Xu, C., and An, Z.: The Air Pollution Caused by the Burning of Fireworks during the Lantern Festival in Beijing. Atmos. Environ. 41, 417-431, https://doi.org/10.1016/j.atmosenv.2006.07.043, 2007.

Webster, H., Visible Spectra of Standard Navy Colored Flares. Propellants, Explos., Pyrotech. 10, 1-4. https://doi.org/10.1002/prep.19850100102, 1985.

Xue, J., Yuan, Z., Lau, A. K. H., and Yu, J. Z.:Insights into Factors Affecting Nitrate in $PM_{2.5}$ in a Polluted High NOx Environment through Hourly Observations and Size Distribution Measurements. J. Geophys. Res.: Atmos. 119, 4888-4902, https://doi.org/10.1002/2013JD021108, 2014.

Zhang, H., Guo, H., Hu, J., Ying, Q., and Kleeman, M. J.: Modeling Atmospheric Age Distribution of Elemental Carbon Using a Regional Age-Resolved Particle Representation Framework. Environ. Sci. Technol. 53, 270-278, https://doi.org/10.1021/acs.est.8b05895, 2019.

Zhang, R., Wang, G., Guo, S., Zamora, M. L., and Wang, Y.: Formation of Urban Fine Particulate Matter. Chem. Rev. 115, 3803-3855, https://doi.org/10.1021/acs.chemrev.5b00067, 2015.

Zhang, H., Worton, D. R., Shen, S., Nah, T., Isaacman-VanWertz, G., Wilson, K. R., and Goldstein, A. H.: Fundamental Time Scales Governing Organic Aerosol Multiphase Partitioning and Oxidative Aging, Environ. Sci. Technol., 49, 9768–9777, https://doi.org/10.1021/acs.est.5b02115, 2015.

Zhao, X., Zhao, X., Liu, P. Chen, D., Zhang, C., Xue, C., Liu, J., and Mu. Y.: Transport Pathways of Nitrate Formed from Nocturnal N_2O_5 Hydrolysis Aloft to the Ground Level in Winter North China Plain. Environ. Sci. Technol. 57, 5108-5118, https://doi.org/10.1021/acs.est.4c02495, 2023.

Zhao, X., Zhao, X., Zhu, W., Liu, Z., and Hu, B.: Formation Dominated by Nocturnal N_2O_5 Hydrolysis in Urban Areas Driven by Regional Atmospheric Transport. Environ. Sci. Technol. 60, https://doi.org/10.1021/acs.est.6c02100, 2026.

Zhong, H., Huang, R.-J., and Lin, C.: Measurement Report: On the Contribution of Long-Distance Transport to the Secondary Aerosol Formation and Aging. Atmos. Chem. Phys. 22, 9513-9524, https://doi.org/10.5194/acp-2022-270, 2022.